Edge-Preserving Ultrasonic Strain Imaging with Uniform Precision

Hossein Khodadadi[1], Amir G. Aghdam[2] and Hassan Rivaz[3]

Abstract— **Ultrasound elastography involves measuring the mechanical properties of tissue, and has many applications in diagnostics and intervention. A common step in different elastography methods is imaging the tissue while it undergoes deformation and estimating the displacement field from the images. A popular next step is to estimate tissue strain, which gives clues into the underlying tissue elasticity modulus. To estimate the strain, one should compute the gradient of the displacement image, which amplifies the noise. The noise is commonly minimized by least square estimation of the gradient from multiple displacement measurements, which reduces the noise by sacrificing image resolution. In this work, we adaptively adjust the level and orientation of the smoothing using two different mechanisms. First, the precision of the displacement field decreases significantly in the regions with high signal decorrelation, which requires increasing the smoothness. Second, smoothing the strain field at the boundaries between different tissue types blurs the edges, which can render small targets invisible. To minimize blurring and noise, we perform anisotropic smoothing and perform smoothing parallel to the direction of edges. The first mechanism ensures that textures/variations in the strain image reflect underlying tissue properties and are not caused by errors in the displacement estimation. The second mechanism keeps the edges between different tissue structures sharp while minimizing the noise. We validate the proposed method using phantom and in-vivo clinical data.**

I. Introduction

Ultrasound elastography reveals mechanical properties of tissue and has numerous applications in both diagnostics and surgical planning [1], [2]. It is usually composed of two separate steps of estimation of a displacement field, followed by inferring mechanical properties from the displacement field. In the second step, it is common to estimate a strain image, which is the spatial derivative of the displacement field and is highly correlated with mechanical properties of tissue. Since differentiation amplifies high frequency noise, most strain estimation techniques combine differentiation with smoothing to increase the signal to noise ratio (SNR) of the strain image. An overview of common techniques for estimating high SNR strain images is provided in [3].

Previous work for estimating the strain field has two major disadvantages. First, it does not take into account the precision of the displacement field. Therefore, a technique for uniform precision strain estimation is introduced in [3], which adaptively increases the level of smoothness in regions with low precision displacement estimates. Second, smoothing blurs boundaries of edges between regions of low and high strain values. A technique for generating sharp strain images that have high SNR is introduced in [4] base on Kalman filtering. This work combines the advantages of these two techniques by introducing a uniform precision edge-preserving strain imaging technique based on bilateral filtering.

Bilateral filtering was first popularized in the computer vision community by Tomasi and Manduch [5] as an alternative to anisotropic diffusion, and has since been applied to many application in computer vision and image processing. It starts with a standard spatial Gaussian kernel, which is then modified based on image intensity values. The idea is that if a neighboring pixel has a very different intensity value compared to the center pixel, its averaging weight is reduced. Therefore, it reduces the noise while preventing over smoothing.

In this work, we adaptively adjust the both the *level* and *orientation* of the smoothing kernel and introduce a novel uniform precision edge-preserving strain imaging technique. Among many different variations of elastography method, we focus on quasi-static elastography [1], [6], where tissue deformation is slow and its dynamical properties can be ignored. However, the techniques that we develop here can also be applied to other variations of elastography.

This paper is organized as follows. In the next section, we provide details of the our uniform precision edge-preserving filter. We then provide experimental results and compare our method against both uniform precision [3] and Kalman filtering [4] strain estimation techniques using both phantom and *in-vivo* patient data. Conclusions and avenues for future work are provided in Section V.

II. Edge-Preserving Filters

The boundary between two different tissue types is an edge in strain image which contains useful information and must be preserved while smoothing. failing to preserve the edges may render small targets inviable. In this section, an overview of bilateral filter as an edge-preserving filter is presented. Bilateral filter is a technique to smooth an image while preserving edges and can be traced back to the nonlinear Gaussian filters in the work of Aurich and Weule [7] or in Tomasi and Manduchi [5] where its name was first coined. Fast versions of this filter using a piecewise-linear approximation in the intensity domain and appropriate subsampling is introduced in [8]. The idea underlying bilateral filter is fairly straightforward, the intensity value at each pixel in an image is replaced by a weighted average of intensity values from nearby pixels as in nearly all smoothing filters. However, unlike others, the weights depend not only

[1,2,3] Authors are with the Department of Electrical and Computer Engineering and PERFORM Centre, Concordia University, Montreal, Quebec, H3G 1M8, Canada. {h_khodad, aghdam, hrivaz}@ece.concordia.ca

on Euclidean distance of pixels, but also on the radiometric differences such as range differences. Similar to the notion of Euclidean distance closeness, intensity similarity in range domain is introduced in bilateral filter and the overall weight of a pixel in the average is computed by multiplying the spatial closeness and range similarity. This makes the filter nonlinear but it preserves sharp edges because although pixels from different sides of the edges may be close in terms of Euclidean distance, but their intensities are not similar. Therefore, they will have small weights in the weighted average. In other words the smoothing will be parallel to the direction of the edge. Note that the term range qualifies quantities related to pixel values like intensities. The formulation of bilateral filter is as follows [5]:

$$I^{BF}(x) = \frac{1}{W_p} \sum_{x_i \in \Omega} I(x_i) f_r(\|I(x_i) - I(x)\|) g_s(\|x_i - x\|) \quad (1)$$

where the W_p is the normalization factor:

$$W_p = \sum_{x_i \in \Omega} f_r(\|I(x_i) - I(x)\|) g_s(\|x_i - x\|) \quad (2)$$

The Ω is the window centered at x and $I(x)$, $I^{BF}(x)$ are the original and filtered image, respectively. Functions f_r and g_s are the range and spatial kernel for smoothing difference in intensities and coordinates, respectively. Gaussian functions are good candidate for the spatial and range kernel as they give a low weight to pixels that are either spatially far or have dissimilarity in photometric range:

$$f_r(x) = G_{\sigma_r}(x) = \frac{1}{2\pi\sigma_r^2} e^{-\frac{x^2}{2\sigma_r^2}} \quad (3)$$

$$g_s(x) = G_{\sigma_s}(x) = \frac{1}{2\pi\sigma_s^2} e^{-\frac{x^2}{2\sigma_s^2}} \quad (4)$$

The bilateral filter with Gaussian functions has two parameters: σ_r and σ_s. The spatial spread σ_s is chosen based on the desired amount of smoothness or low-pass filtering. A large σ_s includes the intensities of pixels from more distant image locations in the domain. Similarly, the photometric spread σ_r in the image range determine how close in range the pixels should be to be considered as similar pixels. Figure 1(a) shows an example of a simple gray-scale image with an edge in the middle which is perturbed by Gaussian noise. Figure 1(b) depicts the result of applying bilateral filter to this image and figure 1(c) shows the kernel of the bilateral filter at a point located on the edge in which it's clear that only the weight of pixels that are located at one side of the edge, are non-zero, therefore the edge will be untouched.

III. Uniform Precision Edge-Preserving Filter

In this section, first a method for calculating the precision is reviewed and then the main contribution of this paper, which is a proper integration of both edge-preserving and uniform precision properties in one filter, is presented.

It was shown in [9] that the precision p of the displacement data can be estimated, under some simplifying assumptions, from complex cross-correlation ρ of matched displacement

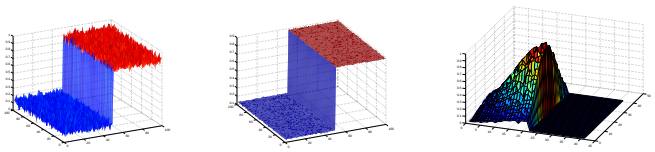

(a) (b) (c)

Fig. 1. (a) Original gray-scale image (b) smoothed Image filtered by bilateral filter (c) Gaussian kernel at the edge of the image $I(50,50)$.

windows of pre- and post-deformation data. The precision $p(x,y)$ and cross-correlation $\rho(x,y)$ can be computed as follows [9]:

$$\rho(\Omega_n, \hat{d}_n) = \frac{\sum_{\{x,y\} \in \Omega_n} I_1(x,y) I_2(x + \hat{d}_n^x, y + \hat{d}_n^y)}{\frac{1}{2} \sum_{\{x,y\} \in \Omega_n} |I_1(x,y)|^2 + |I_2(x + \hat{d}_n^x, y + \hat{d}_n^y)|^2} \quad (5)$$

$$p(x,y) = \frac{\rho(\Omega_n, \hat{d}_n)}{1 - \rho(\Omega_n, \hat{d}_n)} \quad (6)$$

where Ω_n is the displacement window, I_1 and I_2 are the pre- and post-deformation images and $\hat{d}_n^x$, $\hat{d}_n^y$ are the estimated axial and lateral displacement, respectively. In this work, the assumption of negligible lateral displacement in [9] and [3] is released since both axial and lateral displacements are calculated.

Knowing the precision, the goal is to make the smoothing adaptive to the precision of the image while keeping the edges untouched. The adaptation mechanism should blur the regions with low precisions while preserving the regions of high precision. The range kernel is in charge of the edge-preserving function of the filter and should remain untouched. Since the level of smoothing is related to the spatial kernel of the bilateral filter, making the parameter σ_s adaptive to the precision of the image seems to be the logical approach. When the precision is high, the parameter σ_s should be low and vice-versa. The only difficulty that remains is defining the mathematical relation between σ_s and p. Suppose that a Gaussian blur is used to smooth an image, the cut-off frequency of this linear low-pass filter in each direction is $f_c \propto \frac{1}{\sigma_s}$ consequently the resolution in each direction will be $R \propto \sigma_s$ where σ_s is the Gaussian spatial spread. Now, suppose the raw strain data contains independent measurement from the same relatively homogeneous strain distribution, the filtered strain precision will scale with the size of the Gaussian kernel width. Note that the 2D kernel will have a size proportional to the square of the 1D kernel size [3]. Bearing in mind that the kernel size is proportional to spatial spread, If the precision of the original image was p_0, the precision of the smoothed image would be

$$p(x,y) \propto p_0(x,y) \sigma_s^2(x,y). \quad (7)$$

This leads to

$$\sigma_s(x,y) = \frac{k}{\sqrt{p_0(x,y)}}. \quad (8)$$

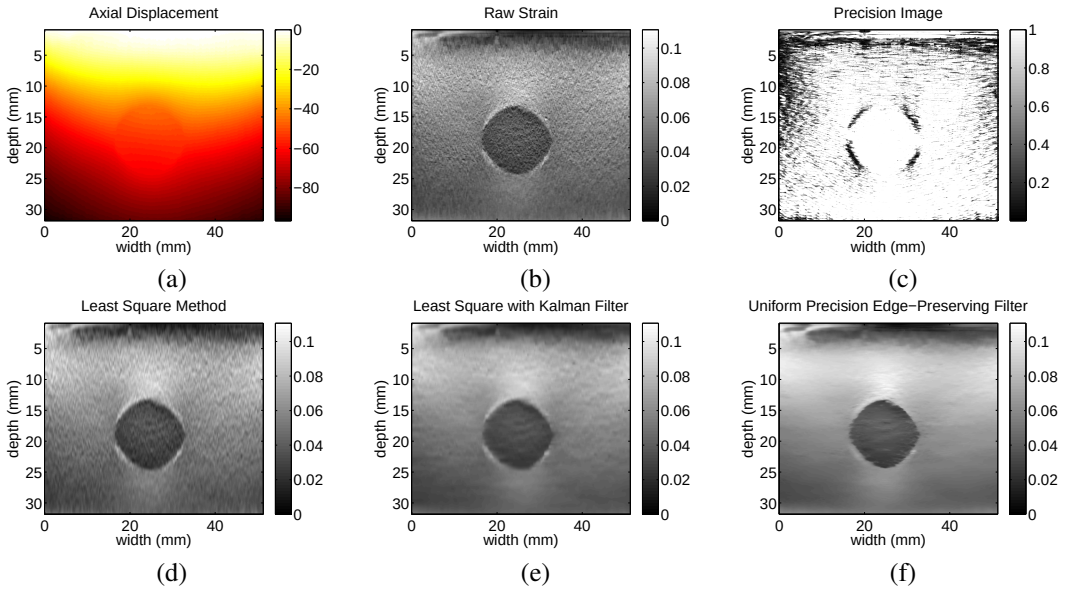

Fig. 2. The result of different methods applied to the phantom data: (a) Axial displacement (b) Raw strain data calculated by simple discreet differentiation of the axial displacement (c) The precision image (d) The result of the least square method applied to the axial displacement (e) The result of the least square method with Kalman filter applied to the axial displacement (f) The result of the proposed uniform precision edge-preserving filter applied to the raw axial strain image

Substituting 8 in 7 will cancel out the initial precision $p_0(x,y)$ from the Eq. 7 and therefore a uniform precision image can be produced. The precision scaling factor k can tune the level of overall precision after smoothing.

The above reasoning for Gaussian blur can be extended to bilateral filter, Since the range kernel does not change spatial kernel size. Note that the computation time of this approach is less than or equal to bilateral filter because the size of kernel is reduced when the image has some degree of precision.

It should be noted that a precision value of zero results in $\sigma_s = \infty$ in .8. In practice σ_s can not be infinity so a maximum spatial spread is defined as σ_{max}, and any value higher than this value is substituted by σ_{max}.

IV. Experimental Results

In this section, phantom results and patient trail are presented. The RF data is acquired from an Antares Siemens system (Issaquah, WA) at the center frequency of 6.67 MHz with a VF10-5 linear array at a sampling rate of 40 MHz. To evaluate the proposed filter first the 2D AM method introduced by Rivaz et. al. [4] is used to produce axial and lateral displacement images from RF data and then the proposed method is applied to the displacement images to calculate the precision and the strain. To compare the results, two other methods are also applied to the data which are as follows:

1) Least square method: the most common approach that is used for generating the strain image from the displacement image. Roughly speaking, the least square method compute the strain in each pixel by calculating the slope of a line fitted to the displacement data of a window in axial direction. To make the strain more accurate, the line window could be a plane in 2D where the strain is calculated for the center of the plane.
2) Least square with Kalman filter: This approach originally proposed by Rivaz et. al. [4], further smooth the result strain of the least square in the lateral direction. The Kalman filter is used because it gives the ability to keep the edges while smoothing the rest of the image.

A Gaussian Blur filter is used to pre-process the strain image and due to the fact that the strain image is produced by calculating the displacement in the axial line the result strain image needs more smoothing in lateral direction so an unsymmetric kernel is used for the filter.

Throughout this section, the parameters of 2DAM are set to $\alpha = 5$, $\beta_a = 10$, $\beta_l = 0.005$ and $T = 0.2$ (Eqs. 12 and 20 in [4]), and the tunable parameters of Dynamic Programming (DP) are $\alpha_\alpha = \alpha_l = 0.15$ (Eq. 1 in [4]). In the precision calculation the window size is $\Omega = 40$, while the spatial and range spreads in bilateral filter are adaptive to the image properties ($\sigma_s = \frac{Width(I)}{10}$, $\sigma_r = \frac{I_{max} - I_{min}}{16}$). Finally, in the proposed filter, the maximum spatial spread is $\sigma_{max} = 30$, the range spread is adaptive with the image ($\sigma_r = \frac{I_{max} - I_{min}}{16}$) and the scaling factor of precision is: $k = 3$.

A. Phantom Data

Figure 2 shows the phantom results obtained from different methods. As one can see, the least square method has produced a somehow smooth strain data with very blurry edges. Moreover the least square with Kalman filter is the same as the least square but more smooth in the lateral direction. It's worth noting that the Kalman filter tried to keep the edges untouched when smoothing in the lateral

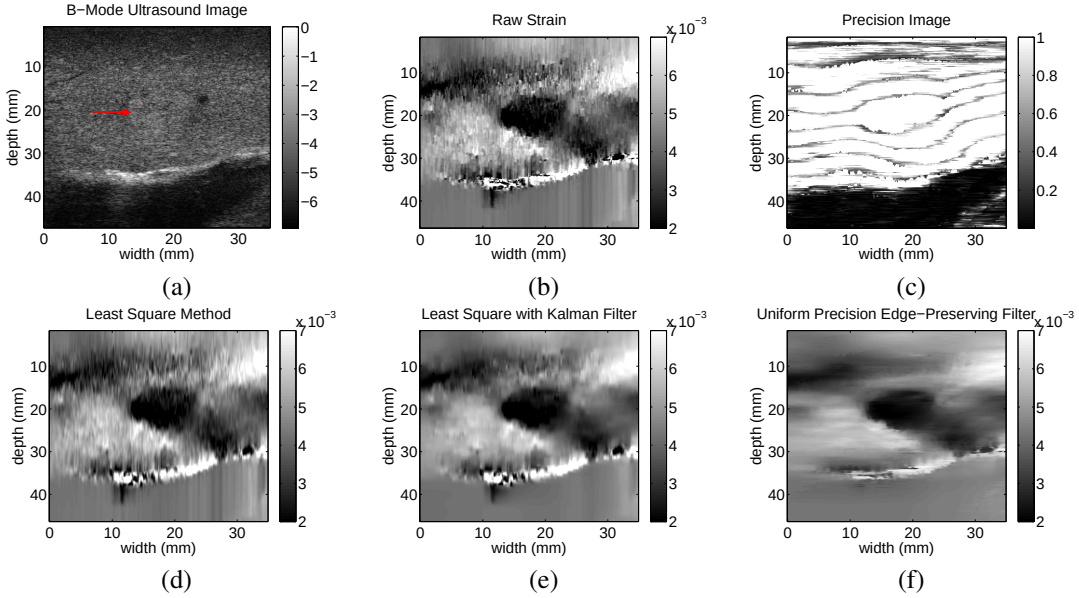

Fig. 3. The result of different methods applied to the patient data: (a) Axial displacement generated (b) Raw strain data calculated by simple discreet differentiation of the axial displacement (c) The precision image (d) The result of the least square method applied to the axial displacement (e) The result of the least square method with Kalman filter applied to the axial displacement (f) The result of the proposed uniform precision edge-preserving filter.

direction. Figure 2(f) depicts the result of the proposed uniform precision edge-preserving filter applied to the raw axial strain image where it is clear that the edges are untouched. The uniform precision properties of the filter is not distinguishable here because the precision of the phantom result is already somehow uniform (Figure 2(c)).

B. In-vivo Data

The data is acquired from patients undergoing open surgical radiofrequency (RF) thermal ablation for primary or secondary liver cancer. The Institution's Ethical Review Board at Johns Hopkins University approved all experimental procedures involving human subjects. Figure 3 shows the ultrasound and strain images of a patient before ablation. A hard tumor, marked with an arrow, is hardly visible in the ultrasound image. The result of applying different methods on this data clearly shows the merits of the proposed uniform precision edge preserving filter. Figure 2(f) offers a more informative and less decisive image for the diagnostic applications, because it smoothes the unreliable noisy regions while keeping the information of the precise regions and the edges untouched.

V. Conclusions

In this paper, we have presented an algorithm that can, under certain assumptions, generate strain images with uniform precision but varying resolution. Uniform precision property ensures that textures/variations in the strain image reflect underlying tissue properties and are not caused by errors in the displacement estimation. The algorithm has also the capability of keeping the edges between different tissue structures sharp while minimizing the noise. This is demonstrated by the phantom and in-vivo clinical data. The results are compared to three common methods in this field which showed the effectiveness of the proposed algorithm, however, further clinical studies will be necessary to assess th benefits of the algorithm.

ACKNOWLEDGMENT

E. Boctor, M. Choti and H. Rivaz collected the patient data at Johns Hopkins Hospital. The authors would like to thank E. Boctor and M. Choti for allowing us to use the data.

References

[1] T. J. Hall, P. Barbone, A. Oberai, and et al., "Recent results in nonlinear strain and modulus imaging," *Current medical imaging reviews*, vol. 7, no. 4, 2011.

[2] O. Mohareri, A. Ruszkowski, J. Lobo, J. Ischia, A. Baghani, G. Nir, H. Eskandari, E. Jones, L. Fazli, L. Goldenberg, M. Moradi, and S. Salcudean, "Multi-parametric 3d quantitative ultrasound vibro-elastography imaging for detecting palpable prostate tumors," in *MICCAI 2014*. Springer, 2014, pp. 561–568.

[3] G. Treece, J. Lindop, A. Gee, and R. Prager, "Uniform precision ultrasound strain imaging," *IEEE Trans. Ultrason. Ferroelectr. Freq. Control*, vol. 56, no. 11, pp. 2420–2436, 2009.

[4] H. Rivaz, E. M. Boctor, M. A. Choti, and G. D. Hager, "Real-time regularized ultrasound elastography," *Medical Imaging, IEEE Transactions on*, vol. 30, no. 4, pp. 928–945, Apr 2011.

[5] C. Tomasi and R. Manduchi, "Bilateral filtering for gray and color images," in *Computer Vision, 1998. Sixth International Conference on*. IEEE, 1998, pp. 839–846.

[6] G. Treece, J. Lindop, L. Chen, J. Housden, R. Prager, and A. Gee, "Real-time quasi-static ultrasound elastography," *Interface focus*, p. rsfs20110011, 2011.

[7] V. Aurich and J. Weule, "Non-linear gaussian filters performing edge preserving diffusion," in *Mustererkennung 1995*, ser. Informatik aktuell, G. Sagerer, S. Posch, and F. Kummert, Eds. Springer Berlin Heidelberg, 1995, pp. 538–545.

[8] F. Durand and J. Dorsey, "Fast bilateral filtering for the display of high-dynamic-range images," *ACM transactions on graphics (TOG)*, vol. 21, no. 3, pp. 257–266, 2002.

[9] J. E. Lindop, G. M. Treece, A. H. Gee, and R. W. Prager, "Dynamic Resolution Selection in Ultrasonic Strain Imaging," *Ultrasound in Medicine and Biology*, vol. 34, no. 5, pp. 809–823, May 2008.